

EM 388F Term Paper: Subcritical Cracking of Low-k Dielectrics

Hualiang Shi

Materials Laboratory for Interconnect and Packing, PRC/MER, Austin, Texas, 78712-1100

Abstract

With the scaling of VLSI, ultra low-k dielectrics with porosity are being introduced to reduce the capacitance coupling. But due to the weak bonding strengths, low-k dielectrics may fail by environmental-assisted subcritical cracking, fracture at stresses far below the loads required for catastrophic failure, causing reliability issues. In this term paper, several references are reviewed to investigate the mechanism of subcritical cracking at multiscale levels.

Various experimental techniques including four point bending (FPB) and double cantilever beam (DCB) were used to evaluate the relationship between crack velocity and energy release rate under environments with different relative humidity (RH), potential of hydrogen (PH), and temperature. It turned out that the graph of crack velocity versus energy release rate was mainly composed of three regions, reaction-controlled region, transport-controlled region, and critical fracture region. Additionally, there was a threshold energy release rate, below which no crack was observed.

In order to understand the physics behind the subcritical cracking, first principle calculations on strained silicate structure were used to investigate how bond strains enhanced the chemical reaction between Si-O bonds and the environments. It showed that by creating Lewis acid sites on silicon and Lewis base site on oxygen, the changes in either Si-O-Si or O-Si-O bond angles increased chemical reactivity.

Introduction of low-k dielectrics

As shown in Fig. 1, the multi-level interconnect structure in ultra-large scale integrated circuits (VLSI) is composed of metal wires and vias, separated by dielectrics [1]. This interconnect structure is used to distribute clock signal and power among circuits on or among chips.

As indicated by Fig. 2, with the scaling of VLSI, the interconnect delay (or RC delay), due to the wire resistance and the capacitance coupling between adjacent wires, is more serious than the gate delay [2].

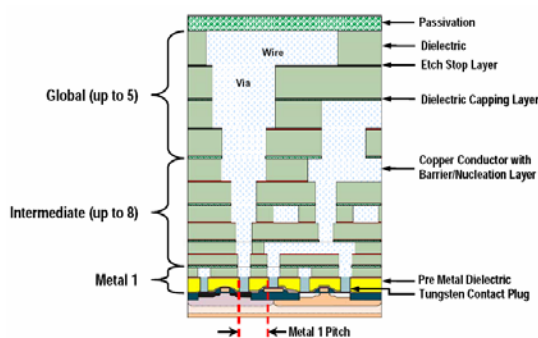


Figure 1. Multi-level interconnect structure

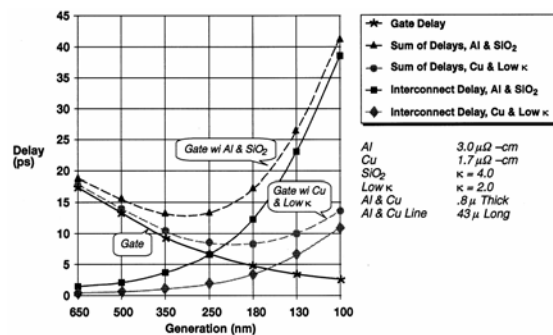


Figure 2. Delay with VLSI scaling

A simple model [3] was created to investigate the mechanism of RC delay, as given in Fig. 3. It turned out that the RC delay is proportional to the wire resistivity and the dielectric constant of insulator. On the basis of this result, copper (Cu) is incorporated to substitute aluminum (Al) because of the lower resistivity and better electromigration property of Cu [4], and low dielectric constant materials are introduced to replace traditional SiO₂ due to the lower dielectric constant.

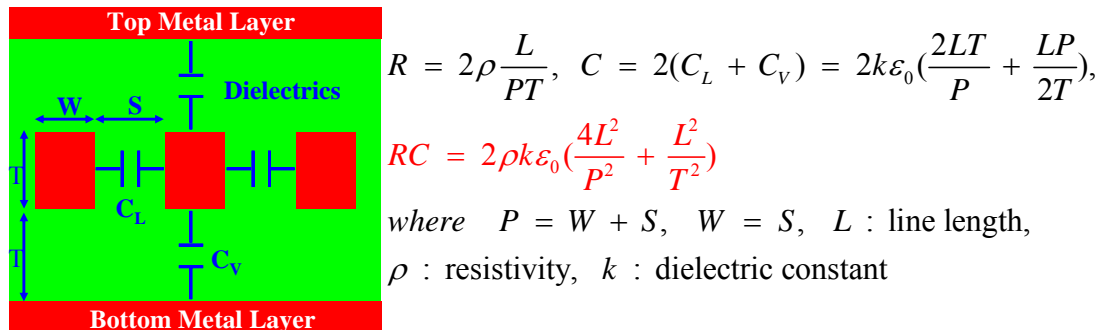


Figure 3. A model for RC delay

According to Clausius-Mossotti-Debye equation,

$$\frac{\varepsilon - 1}{\varepsilon + 2} = \frac{1}{3\varepsilon_0} \left[N_e \alpha_e + N_i \alpha_i + N_o \frac{p_o^2}{3kT} \right],$$

the dielectric constant (ε) is composed of three parts, originating from electronic polarization ($N_e \alpha_e$), ionic polarization ($N_i \alpha_i$), and dipolar polarization ($N_o p_o^2 / 3kT$), where $N_{e,i,o}$ is the density, $\alpha_{e,i}$ the polarizability, p_o the permanent dipole moment, and T the temperature. This equation suggests several approaches to fabricate low k dielectrics. The first method is to reduce polarization, such as the incorporation of $-CH_3$ due to the weaker polarizability of C-H and Si- CH_3 relative to Si-O. The second method is to reduce the density, including the incorporation of terminal organic groups and introduction of air-gap [5, 6, 7].

Due to the process compatibility, Organosilicate low k dielectrics (OSG) have been selected as the low k candidates. A. Grill, etc., studied the bond configurations of OSG by Fourier transform infrared spectroscopy (FTIR) [8]. It turned out that the backbone of OSG is Si-O-Si tetrahedral structure, including cage (1135 cm^{-1} , $\sim 150^\circ$), network (1063 cm^{-1} , $\sim 140^\circ$), and suboxide (1023 cm^{-1} , $< 140^\circ$), as indicated by Fig. 4. J. M. Jacques, etc., investigated the relationship between mechanical properties and bond configurations of OSG [9]. It turned out that with the increase of electron beam (EB) curing time, both the hardness and the modulus were increased, as shown in Fig. 5. At the same time, the Si-O-Si network structure increased and Si-O-Si suboxide structure decreased. So the more the Si-O-Si network structure, the higher the hardness and modulus.

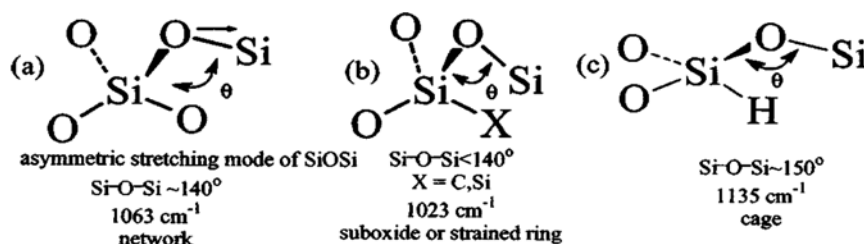


Figure 4. Variation of Si-O-Si bond angle in OSG

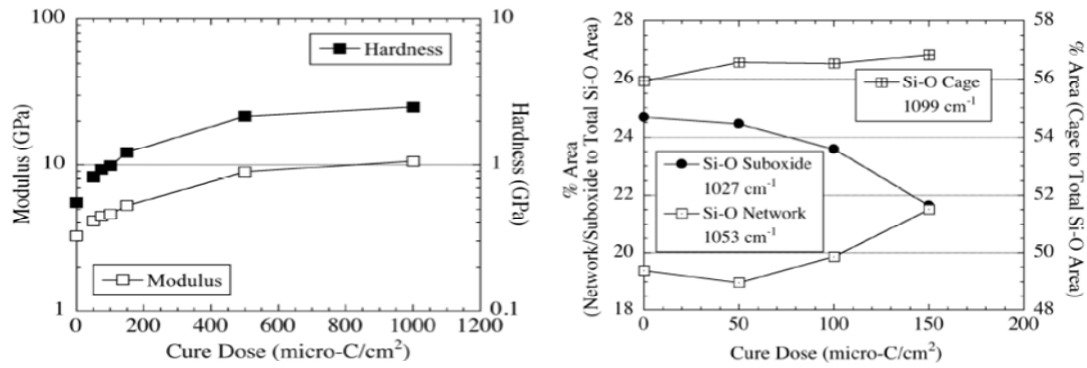


Figure 5. Mechanical property and bond configurations

Although low-k dielectrics are promising, some challenges exist and postpone the implementation of low-k dielectrics [10, 11]. First, there are some process related issues. For example, during the plasma ashing, etching, and cleaning processes, some damages can happen to the sidewall, including carbon depletion, surface hydrophilization, and surface densification. These plasma damages can increase the effective dielectric constant and leakage current, limiting the further scaling of low-k structure. Second, with the decrease of k , the elastic modulus, hardness, and cracking resistance (cohesive strength) decrease. This material issue is further aggravated by stress corrosion, degradation of the material resistance against cracking under the combined influence of stress and environment such as relative humidity (RH) and potential of hydrogen (PH). The driving force might be residual stresses, thermomechanical cycling, and mechanical or vibrational loading. The environment will assist the bond breakage or lower the debonding driving energy by chemical reaction with the low-k backbone structure, Si-O-Si bond configurations.

R. F. Cook, etc., studied the stress-corrosion of HSSQ, as indicated by Fig. 6. The initial crack was induced by Vickers pyramid indenter. After exposure to water, the crack propagated at certain direction and velocity [12]. In Fig. 7, a typical graph for the relationship between crack velocity and energy release rate is given [13, 14, 15]. The following is the summarization for this graph:

- i) There is a **threshold energy release rate**, below which there will be no crack growth.
- ii) If the driving force or energy release rate is low, but higher than the **threshold energy release rate**, the environment or reactants can be transported to the crack tip on time. The limiting factor is the rate of chemical reaction between environment and Si-O-Si bond at the crack tip. This region is usually named as **region I, reaction-controlled region**. In **region I**, crack velocity increased rapidly with the energy release rate.
- iii) If the driving force or energy release rate is high enough, the environment or reactants can not follow up with the crack tip. The limiting factor is the transportation of environment or reactants to the crack tip. This region is named as **region II, transport-controlled region**. In **region II**, crack velocity is almost independent of energy release rate, but strongly dependent on environment.
- iv) If the driving force or energy release rate is too high, critical crack or catastrophic failure happened. This region is called **region III**. In **region III**, the crack velocity is independent of energy release rate.

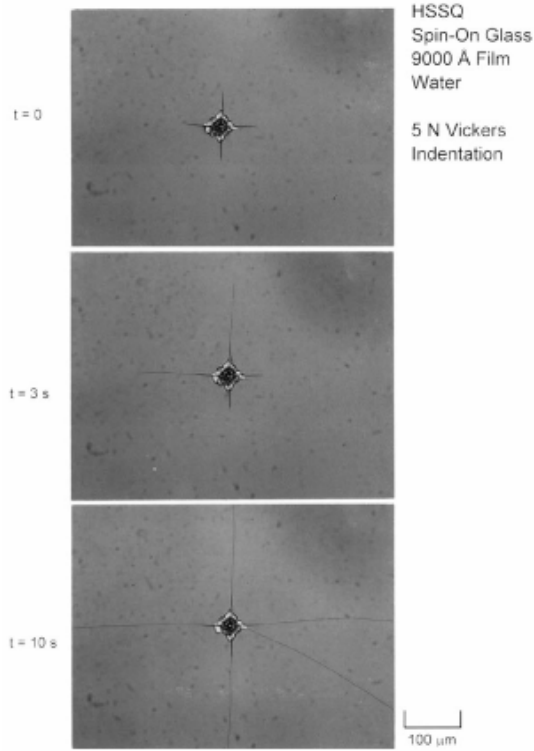


Figure 6. Optical micrograph of crack initiation and propagation in HSSQ exposed to water

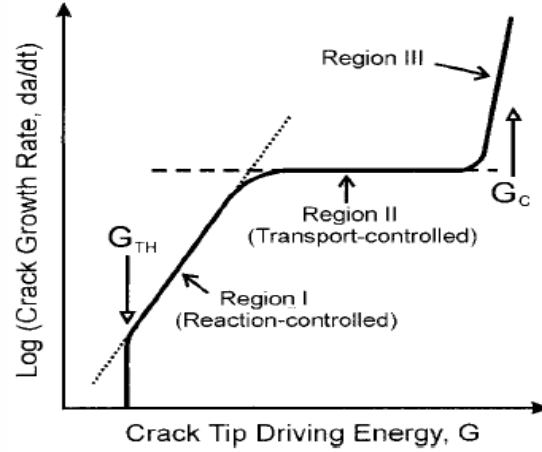


Figure 7. Typical graph of crack velocity vs. energy release rate.

Experiment

J. J. Vlassak used four-point bending test (FPB) to evaluate the relationship between energy release rate and crack velocity [15]. Fig. 8 is the schematic graph for FPB. The energy release rate at the crack tip is:

$$G = \frac{21P^2l^2(1 - \nu^2)}{16Eb^2h^3}$$

where E is the elastic modulus of Si, ν the Poisson's ratio of Si, P the load, l the distance between the inner and outer loading points, b the width of the specimen, and h the substrate thickness.

S. Kook employed sandwiched double cantilever beam (DCB) specimen to measure the subcritical crack growth rate [13]. Fig. 9 is the representative of the DCB test. The energy release rate is:

$$G = \frac{12P^2a^2}{W^2h_1^3E_1'} \left[1 + \frac{2}{Ch_1^{0.25}} \left(\frac{h_1}{a} \right) + \left(\frac{1}{C^2h_1^{0.5}} + \frac{E_1'}{8\mu_1} \right) \cdot \left(\frac{h_1}{a} \right)^2 \right]$$

$$C = \left(\frac{3k}{E_1'W} \right)^{0.25}, \quad k = \frac{4WE_1'E_2'}{h_1E_2' + 4h_2E_1'(1 - \nu_2'^2)},$$

$$E' = \frac{E}{1 - \nu^2}, \quad \nu_2' = \frac{\nu_2}{1 - \nu_2}$$

where P is the applied load, a the crack length, h_1 the half beam height, h_2 the half thickness of polymer film, W the thickness, E_1 the elastic modulus of substrate, E_2 the elastic modulus of polymer film, ν_1 the Poisson's ratio of substrate, ν_2 the Poisson's ratio of polymer film, and u_1 the

shear modulus of the substrate.

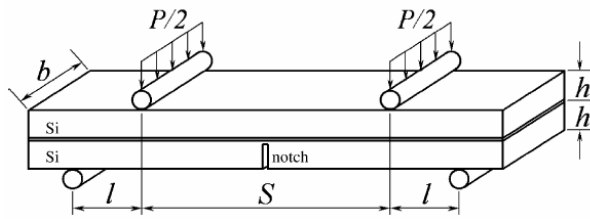


Figure 8. Four point bend test (FPB)

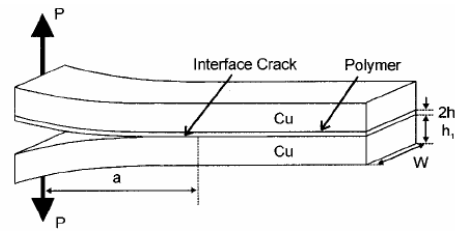


Figure 9. Double cantilever beam test (DCB)

As shown in Fig. 10, Gaussian software can be used for quantum chemistry calculation [16]. There are several input parameters such as initial guess geometry, model theory (**DFT**, etc.), basis set (**6-31 G(d)**, etc.), keyword (**Opt** for geometry optimization), multiplicity of the molecule (spin), and charge of the molecule (0, etc.). Gaussian software is powerful because it can provide a lot of outputs such as the optimum geometry, dipole moment, vibrational frequency, total energy, transition state, and spectra (FTIR, UV, and NMR).

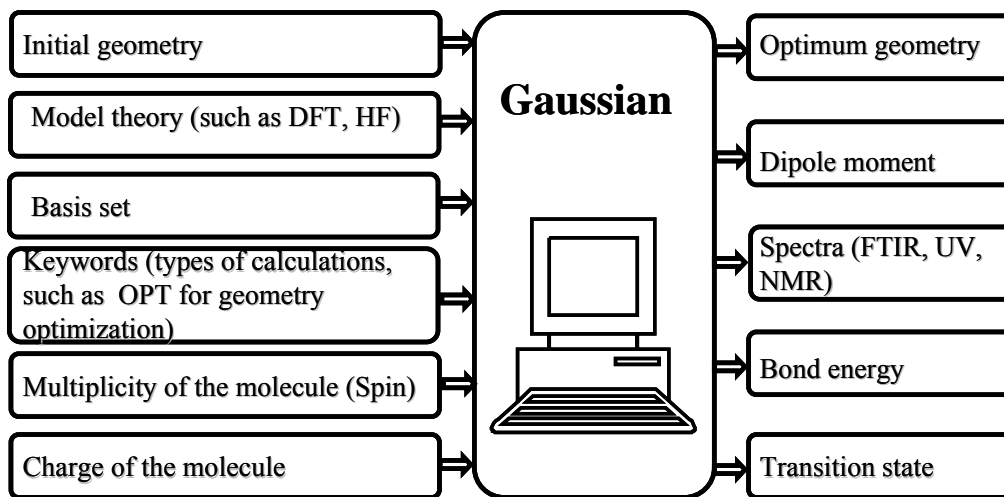


Figure 10. Implementation of quantum chemistry calculation.

Mechanistic study of subcritical crack

i) **Region I:**

Based on the kink motion model by Lawn, J. J. Vlassak did the following analysis [15]:

$$A + nX \leftrightarrow AX_n^* \leftrightarrow B$$

$$\Delta F = (\mu_B - \mu_A - n\mu_X)N = 2\gamma$$

$$\Delta \overline{G}^* = \Delta \overline{G}_0^* - \frac{\beta G}{N}, \quad \Delta \overline{G}^* = \Delta \overline{G}_0^* + \frac{(1 - \beta)G}{N}$$

$$\omega = \omega_0 \left\{ \exp\left(-\frac{\Delta \overline{G}^*}{kT}\right) - \exp\left(-\frac{\Delta \overline{G}^*}{kT}\right) \right\}$$

$$v = v_0 \sinh\left(\frac{G - 2\gamma}{2NkT}\right)$$

where A means an unbroken Si-O-Si bond, X environment or reactant, n the number of reactant involved in the reaction, AX_n^* the transition state, B the reaction product, F the

Gibbs free energy, μ the chemical potential, N the bond density, γ the surface energy, G energy release rate, β a constant reflecting the asymmetry of the energy barrier (assumed to be 0.5), k the Boltzmann constant, T the temperature, and v the crack velocity.

ii) **Region II:**

In ambient environment, when the crack openings are bigger than the mean free path, transportation of reactants can be regarded as fluid flow. But if the crack opening is smaller than the mean free path, the collision between reactants and crack surfaces will happen. So around the crack tip, the transportation of reactants can be characterized as molecular flow. The following is the crack velocity [15]:

$$v_1 = \frac{64(1 - v^2)Gp_x}{3\pi nNE\sqrt{2\pi m_x kT} \ln(l/b)}$$

where p_x is the partial pressure of the reactant x , m_x the molecular mass of reactant x , l the mean free path, n the number of reactant involved in the reaction, E the Young's modulus of solid, ν the Poisson's ratio of solid, G the mode I energy release rate.

In aqueous environment, there are several situations. First, if the crack velocity is slow, the liquid can follow the crack tip. In this case, the diffusion of reactant in the liquid is the limiting factor. Second, if the crack velocity is too fast, the fluid can not keep up with the crack tip. So a bubble or cavitation will be formed around the crack tip, as shown in Fig. 11. In this case, the reactant will reach the crack tip by surface diffusion along the crack surface. The following are some possible solutions:

$$p(x) = p_a - \frac{3\pi\mu v_3 E}{8G(1 - v^2)} \ln\left(\frac{c}{x}\right)$$

$$v_3 = \zeta \frac{8G(1 - v^2)p_a}{3\pi\mu E} \sim 10^{-3} \text{ m/s}$$

where p_a is the ambient fluid pressure, x the distance from the crack tip, c the crack length, and ζ a numerical constant.

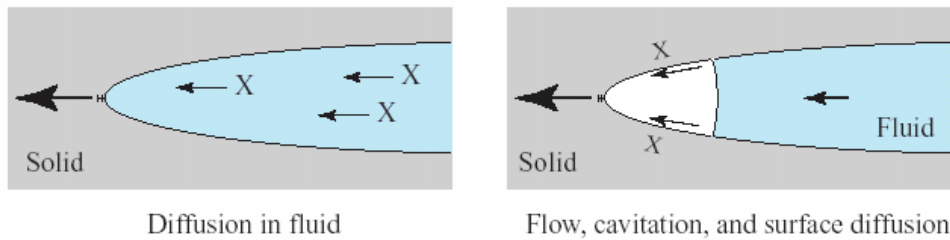
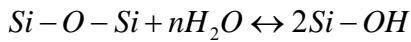


Figure 11. Possible limiting transportation mechanisms in aqueous environment.

iii) Influence of **RH**:

J. J. Vlassak evaluated the RH effect on subcritical crack growth of OSG/TaN. As shown in Fig. 12, the crack velocity data was well fitted by the model in region I, $v = v_0 \sinh\left(\frac{G - 2\gamma}{2NkT}\right)$. The bond density, N , was approximated to be $8 \times 10^{18} \text{ m}^{-2}$. For the same energy release rate, the crack velocity increased with RH. Additionally, the threshold

energy release rate shifted to the lower value with the increase of RH. In Fig. 13, a linear relationship between threshold energy release rate and the natural logarithm of the water partial pressure was given. It can be explained by the following equations:



$$2\gamma = N(2\mu_{Si-OH} - \mu_{Si-O-Si} - n\mu_{H_2O}) = N[\Delta\mu - nkT \ln p_{H_2O}]$$

The slope will provide the value of n, the number of water molecules involved in the Si-O-Si bond breakage. In this case, n was approximated to be 10, which was a little bit big and needed to further check.

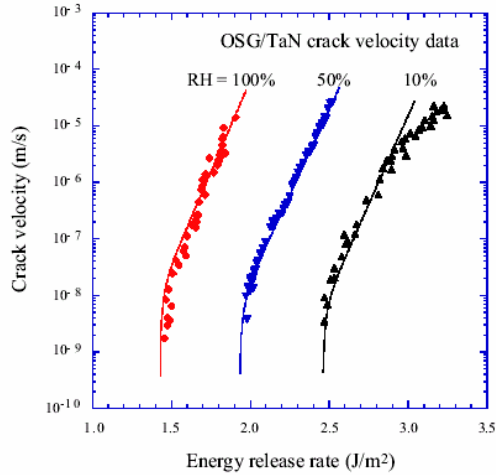


Figure 12. Subcritical crack growth in ambient environment.

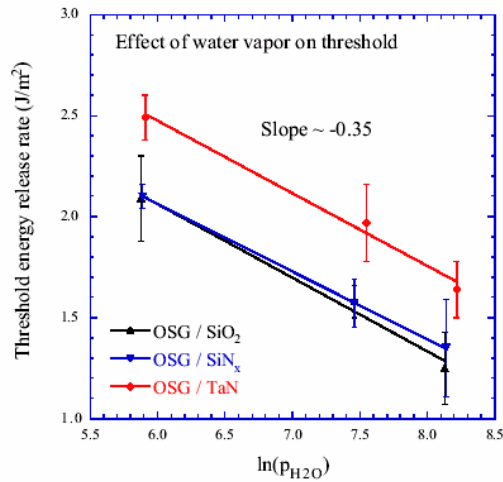


Figure 13. Threshold energy release rate vs. Partial pressure of water vapor.

S. Kook also investigated the RH effect on stress corrosion [13]. As shown in Fig. 14, the subcritical crack included both region I and region II. Region I can be fitted well by

$$v = v_0 \sinh\left(\frac{G - 2\gamma}{2NkT}\right) \text{ and region II can be represented by } v = \frac{HD_{H_2O}}{L} \left(\frac{P_{H_2O}}{P_0}\right),$$

where H is a constant, D_{H_2O} the water diffusion coefficient, and L the length of stagnant region from the crack tip. It turned out that the crack velocity in region II was linearly dependent on the partial pressure of water vapor.

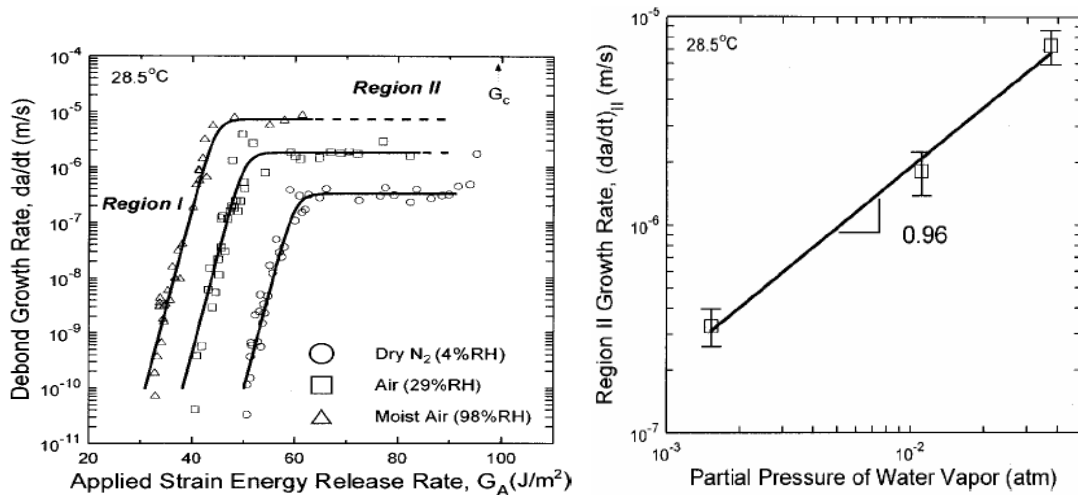


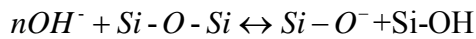
Figure 14. Stress corrosion with different RH.

iv) Influence of **PH**:

In the same paper, J. J. Vlassak also studied the PH effect on subcritical crack growth of OSG/SiN_x. As shown in Fig. 15, the subcritical crack was well fitted by the model in region I, $v = v_0 \sinh\left(\frac{G - 2\gamma}{2NkT}\right)$. For the same energy release rate, the crack velocity increased with PH. Additionally, the threshold energy release rate shifted to the lower value with the increase of PH. Moreover, the slope decreased with the increase of PH, probably due to the change of crack tip radius or change of reaction activation volume induced by PH. In Fig. 16, a linear relationship between threshold energy release rate and PH was given. It can be explained by the following equations:

$$I, v = v_0 \sinh\left(\frac{G - 2\gamma}{2NkT}\right)$$

$nOH^- + Si - O - Si \leftrightarrow Si - O^- + Si-OH$
 $2\gamma = N[\Delta\mu + 14nkT \ln 10 - nkT \ln 10 pH]$



$$2\gamma = N[\Delta\mu + 14nkT \ln 10 - nkT \ln 10 pH]$$

The slope will provide the value of n, the order of reaction. In this case, n was approximated to be 0.56 ± 0.07 .

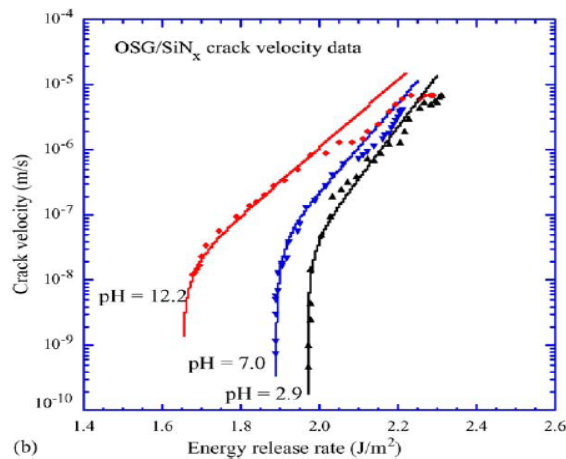


Figure 15. Subcritical crack growth with different PH.

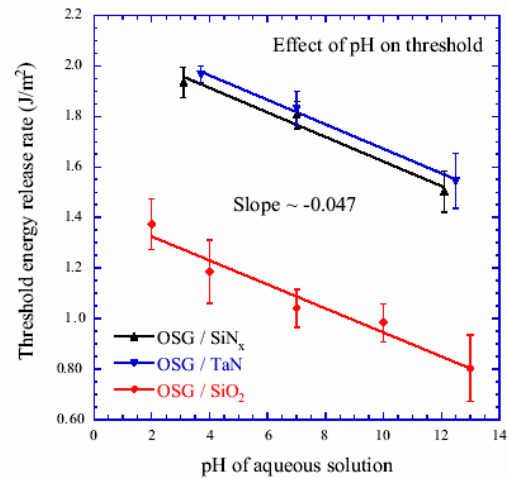


Figure 16. Threshold energy release rate vs. PH.

Quantum chemical study of subcritical cracking

T. A. Michalske did some mechanistic study about the interaction between water or acid and the strained Si-O-Si bond [17]. A three-step Michalske-Freiman (MF) Model was proposed, as indicated by Fig. 17.

- i) A water molecule was adsorbed on the crack tip by the share of electron lone pair between Si atom and the oxygen atom from water, and the share of electron lone pair between bridging oxygen atom and the proton from water.
- ii) Bond breakage of Si-O bond and O-H bond from adsorbed water and formation of two silanol bonds, connected together by hydrogen bond.
- iii) Bond breakage of hydrogen bond and formation of two silanol bonds.

Additionally, T. A. Michalske also used molecular-orbital method to study how bond strain enhanced the reactivity between water and Si-O-Si bond. The basic idea was from the calculation of electron distribution under the influence of different strain. The strength of Si-O bond was determined by the electron distribution or the bond overlap populations. Additionally, the higher

the charge density of Si atom or bridging oxygen atom, the higher ionic attraction or covalent interaction to polar molecules such as water. As indicated by Tab. 1, when the Si-O-Si angle was smaller than 120°, the bond overlap population between Si and bridging oxygen atom was reduced to 0.143, charge on Si was increased to 2.89, and charge on bridging oxygen was increased to -1.47. So when Si-O-Si angle was below 120°, the reactivity was increased significantly.

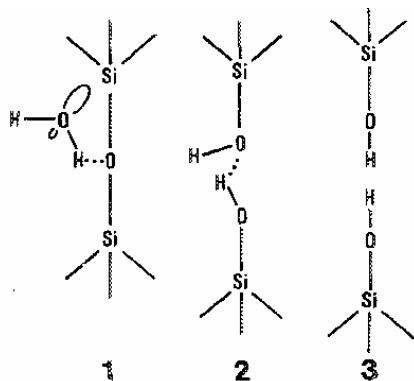


Figure 17. A three-step Michalske-Freiman (MF) Model.

Table I. Electron distribution for strained Si-O bonds.

d^a	ϕ^b	$n(\text{Si-O}_{br})^c$	$Q(\text{Si})^d$	$Q(\text{O}_{br})^e$	$e^-[\text{O}_{nbo}]^f$
1.62	140°	0.550	1.36	-0.66	-3.5
1.62	180°	0.579	1.38	-0.70	-4.0
1.57	180°	...	1.40	-0.72	-3.84
1.67	180°	...	1.36	-0.68	-4.10
1.57	140°	...	1.38	-0.69	...
1.67	140°	...	1.33	-0.63	...
1.62	110°	0.502
1.62 ^g	90°	0.143 ^g	2.89 ^g	-1.47 ^g	...

^a Bond distance.

^b Bond angle ($\theta = \text{O-Si-O}$ bond angle = 109° for entire table).

^c Bond overlap population between Si and the bridging oxygen.

^d Atomic charge on Si.

^e Atomic charge on bridging oxygen.

^f Electron density in lone pair orbitals of the bridging oxygen.

^g Calculated for edge-shared tetrahedral geometry.

M. Cypryk used quantum chemistry method to study the effect of number of water molecules on the reaction between water and disiloxane [18]. As indicated by Fig. 18, the general procedure included the optimization of initial geometry for reactant and the calculation of transition state and product. The key idea was to evaluate the activation energy, which was the energy difference between transition state and reactant. The reactivity was determined by Arrhenius equation:

$k = Ae^{-\frac{E_a}{RT}}$, where k is the rate coefficient, A a constant, E_a the activation energy for the chemical reaction between water and Si-O-Si bond, R the universal gas constant, and T the temperature.

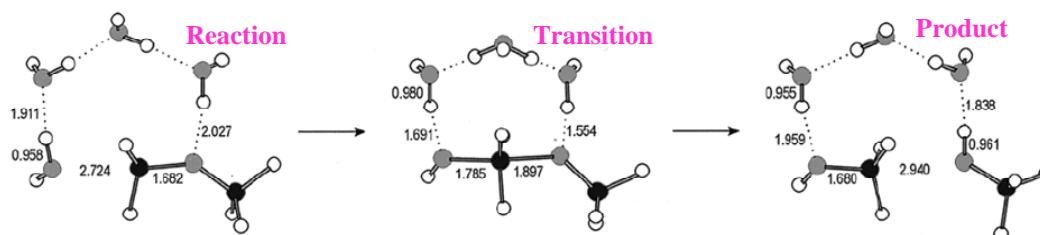


Figure 18. General procedure for the calculation of transition state.

In Fig. 19, the transition states for the interaction between disiloxane and one, two, or four

water molecules were given. The activation energy related to one, two, and four water molecules were 33.9 kcal/mol, 24.7 kcal/mol, and 24.0 kcal/mol. So activation energy decreased with the increase of number of water molecule.

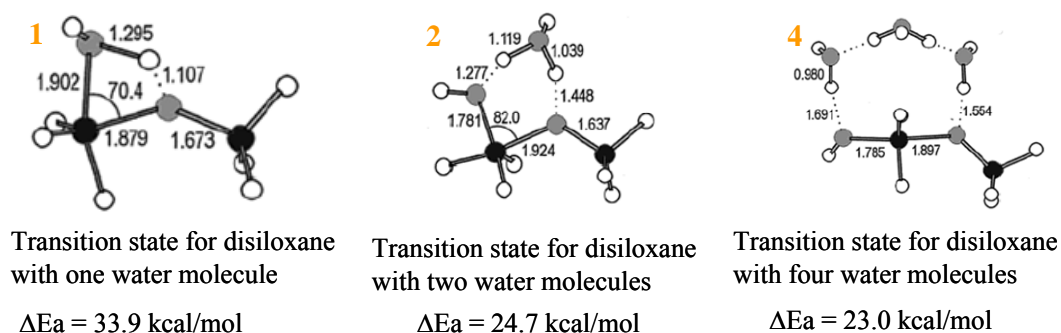


Figure 19. Transition states for disiloxane with different number of water molecules

T. R. Walsh used similar ideas to study the effect of surface defect (or dangling bond) on the reaction between water and disiloxane with one dangling bond. As shown in Fig. 20, if the water molecule was initially adsorbed on the perfect Si atom which had no dangling bond, the activation energy was 120.8 Kcal/mol; however, if the water molecule was initially adsorbed on the defect Si atom which had one dangling bond, the activation energy was 96.0 Kcal/mol. So lower activation energy for reaction around defect site.

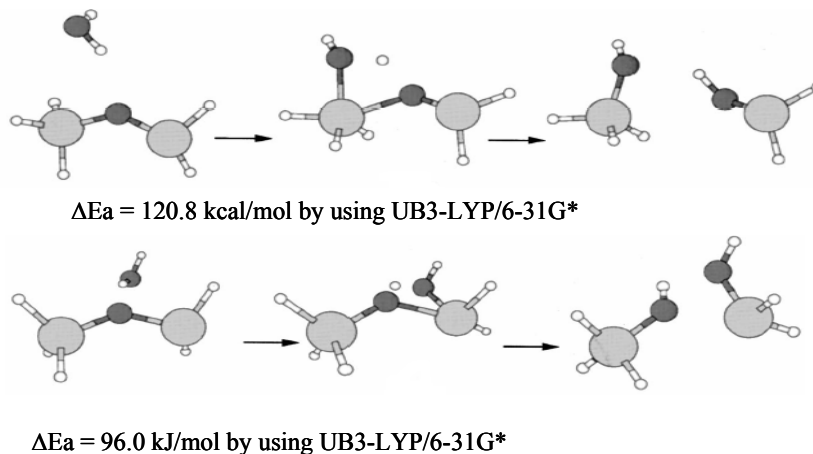


Figure 20. Reactions between water and disiloxane with one dangling bond.

Summary

The graph of crack velocity versus energy release rate was mainly composed of three regions, reaction-controlled region, transport-controlled region, and critical fracture region. Additionally, there was a threshold energy release rate, below which no crack was observed.

First principle calculation was used to investigate how bond strains enhanced the chemical reaction between Si-O bonds and the environments. It showed that by creating Lewis acid sites on silicon and Lewis base site on oxygen, the changes in either Si-O-Si or O-Si-O bond angles increased chemical reactivity. Additionally, both the number of water molecules involved in the reaction and defect site influenced the reactivity.

Reference

1. ITRS 2003 Interconnect, P8.
2. Mark Bohr, IEEE IEDM Proc. 1995.
3. S.P. Jeng, et al, VLSI Tech. Symp. Tech.Dig. (1994) p73.
4. R.Rosenberg, D.C.Edelstein, C. K. Hu, and K. P. Rodbell, Annu. Rev. Mater. Sci., Vol. 30, 229-262 (2000).
5. M. Morgen, E. T. Ryan, J. Zhao, C. Hu, T. Cho, and P. S. Ho, Annu. Rev. Mater. Sci., Vol. 30, 645-680 (2000).
6. K. Maex, M. R. Baklanov, D. Shamiryan, F. Lacopi, S. H. Brongersma, and Z. S. Yanovitskaya, Journal of Applied Physics, Vol. 93, 8793-8840 (2003).
7. H. Shi, J. Bao, J. Liu, H. Huang, R. S. Smith, Q. Zhao, P. S. Ho, M. D. Goodner, M. Moinpour, and G. M. Kloster, the Advanced Metallization Conference (AMC) 2007 Proceedings, VB.3
8. A. Grill and D. A. Neumayer, J. Appl. Phys., 94, 6697 (2003).
9. J. M. Jacques, T. Y. Tsui, and R. Kraft, etc. Mater. Res. Soc. Symp. Proc. Vol. 863 B3.8.1 2005
10. R. J. O. M. Hoofman, et al., Microelectronic Engineering 80 (2005) 337-344.
11. P. S. Ho, lecture note, the University of Texas at Austin, Spring 2008.
12. R. F. Cook, and E. G. Liniger, Journal of the Electrochemical Society, 146(12)4439-4448 (1999).
13. S. Kook and R. H. Dauskardt, J. Appl. Phys., Vol. 91, 1293-1303, 2002.
14. R. Huang, lecture note, the University of Texas at Austin, Spring 2008.
15. J. J. Vlassak, etc., Materials Science and Engineering A 391 (2005) 159-174.
16. H. Shi, qualify examination, the University of Texas at Austin, Fall 2005.
17. T. A. Michalske and B. C. Bunker, J. Appl. Phys. 56 (10) (1984) 2686-2693.
18. M. Cypryk, and Y. Apeloig, Organometalics 2002, 21, 2165-2175.
19. T. R. Walsh, M. Wilson, and A. P. Sutton, J. Chem. Phys. Vol. 113, No. 20, 9191-9201 (2000).